Physics and Chemistry of Minerals (2024) 51:40
https://doi.org/10.1007/s00269-024-01299-0

ORIGINAL PAPER

Interaction of platinum with antimony-bearing compounds in NaF fluids at 800 °C and 200 MPa

Alexander F. Redkin[1] · Andrey M. Ionov[2] · Alexey N. Nekrasov[1] · Andrey D. Podobrazhnykh[3] · Rais N. Mozhchil[2]

Received: 14 August 2024 / Accepted: 11 October 2024

Abstract

Studies conducted in NaF-containing hydrothermal fluids have shown that the oxide compounds Sb^{5+} are unstable at 800 °C, P_{total} = 200 MPa and fO_2 (fH_2) specified by Co–CoO and Ni–NiO buffers interact with the Pt material of the ampoule, forming antimony intermetallics with platinum on the inner surface of the ampoule. The formation of the following intermetallics was established through the analysis of data obtained from studies conducted on an electronic microscope: $Pt_{90.3\pm0.8}Sb_{9.7}$ (~$Pt_{10}Sb$), $Pt_{82.8\pm1.3}Sb_{17.2}$ (~Pt_5Sb) and $Pt_{69.2\pm4.4}Sb_{30.8}$. $Pt_{10}Sb$ compound which was obtained on the inner surface of the Pt ampoule is the limiting solid solution of antimony in platinum at 800 °C. It exhibits a cubic crystal system $Fm\bar{3}m$ with a lattice constant of $a = 3.943(3)$ Å and forms an underdeveloped surface <111>. Pt_5Sb compound, presumably hexagonal *P6/mmm* crystal system with unit cell parameters $a = b = 4.56(4)$, $c = 4.229(2)$ Å, $\alpha = \beta = 90°$, $\gamma = 120°$, forms a thin film (≤ 10 μm) on the Pt surface and appears to be a metastable phase. The intermetallic compound of $Pt_{69}Sb_{31}$ is a rapidly cooled melt of appropriate composition.

A mechanism for deep penetration of Sb into the walls of the Pt ampoule is proposed.

Keywords Hydrothermal experiment · Roméite · Fluorite · Antimony · Platinum · Intermetallic · Sodium fluoride solution · Rebinder effect

Introduction

Antimony, which has an electronic configuration of $4d^{10}$ $5s^2$ $5p^3$, can have oxidation states of -3, 0, +3 and +5 in chemical compounds. The high affinity for sulfur and oxygen means that the main ore minerals of antimony are complex sulfides and oxides which precipitate from hydrothermal solutions containing thio- or halide complexes Sb^{3+} or Sb^{5+} when physico-chemical parameters (T, P, fO_2, fS_2) are altered. As a rule in nature, the precipitation of antimony minerals occurred at $T \leq 400$ °C; the solutions themselves had a distant paragenetic relationship with Al-Si-melts, so in this case behavior of this element at the temperatures of hydrothermal-magmatic activation was not considered. At the same time, it was previously shown (Redkin et al. 2020) that in fluoride solutions containing calcium and sodium, in an oxidizing environment at 800 °C and a pressure of 200 MPa, a complex fluoride oxide belonging to the pyrochlore group, roméite, $CaNaSb_2O_6F$ is stable. This mineral, at $fO_2 = 50$ Pa, specified by the Cu_2O–CuO buffer, has a significant apparent solubility from 0.4 to 2.1 wt% Sb (Redkin et al. 2024) in the fluid immiscibility region of the NaF-H_2O system. In a reducing environment ($fO_2 \leq 10^{-3.47}$ Pa), roméite is not stable, Sb^{5+} is reduced in solution and deposited on the surface of the Pt ampoule. According to preliminary XRD and SEM studies, the newly formed compound is an intermetallic compound of platinum and antimony with the composition Pt_5Sb, hexagonal system

Alexander F. Redkin
redkin@iem.ac.ru

Andrey M. Ionov
ionov@issp.ac.ru

Andrey D. Podobrazhnykh
andrew.podobrazhnykh123@gmail.com

[1] Academician D.S. Korzhinskii Institute of Experimental Mineralogy RAS, 4 Academician Ossipyan str, Chernogolovka, Moscow District 142432, Russia

[2] Institute of Solid State Physics RAS, 2 Academician Ossipyan str, Chernogolovka, Moscow District 142432, Russia

[3] Geology Department of the M.V. Lomonosov Moscow State University, Moscow, Russia

Published online: 28 October 2024

with lattice parameters (LP): $a=b=4.56$ (4), $c=4.229(2)$ Å, $\alpha=\beta=90°$, $\gamma=120°$. Previously, cubic (Durussel and Feschotte 1991) and tetragonal (Kim 1993) structures were attributed to the Pt_5Sb compound. Therefore, the hydrothermal formation and study of the structural features of Pt_5Sb and other intermetallic compounds of platinum and antimony are of great scientific interest.

Previous studies

The stability of intermetallic compounds in the Pt-Sb system has been studied both experimentally (Nemilow and Woronow 1936; Hansen 1936; Bhan et al. 1969; Kim and Chao 1990; Durussel and Feschotte 1991; Kim 1993) and thermodynamically (Liu et al. 2013). The phase diagram in the Pt-Sb system has been the subject of independent expert studies (Okamoto 1992; Itkin and Alcock 1996), which have qualified the results in the temperature range between 500 and 1769 °C (T_{melt} of Pt). The data indicate that at 800 °C and a pressure of 1 bar (10^5 Pa), the stable phases are a solid solution of antimony (up to 10 at% Sb) in platinum and a melt containing, according to various sources, from 26 to 36 at% Sb, PtSb, $PtSb_2$ compounds and platinum melt in antimony from 0 to 5 at% Pt. In numerous earlier research studies (Nemilow and Woronow 1936; Hansen 1936; Hansen and Anderko 1958; Bhan et al. 1969), furthermore, the reference book (Lyakishev 2000), do not address the potential for the formation of antimony penta-platinate in the Pt-Sb system at temperatures exceeding 500 °C. The occurrence of the melt is reported to begin at a Sb concentration of 30 at%. The Pt_5Sb or $Pt_{83}Sb_{17}$ phase has been identified in synthetic products (duration for several days up to 3 months in quartz ampoules) at 600 and 650 °C (Kim and Chao 1990; Kim 1993) (PDF 46-1065). X-ray studies indicate that the phase is similar to the previously described Pt_4Sb and $Pt_{4+x}Sb$, showing a yellowish-gray color and a tetragonal system with unit cell parameters of $a=3.948(1)$, $c=16.85(1)$ Å. The phase is stable up to 755 °C. This allowed for the diagram presented by (Bhan et al. 1969) to be refined. Concurrently, the findings of the Swiss research team (Durussel and Feschotte 1991) were released, which highlighted that the Pt_5Sb compound, characterized by a face-centred cubic structure (fcc), is a solid solution comprising between 15.5 and 18.9 at% Sb. Furthermore, the findings indicated that this compound exhibits stability within a temperature range of 560 to 748 °C. The phase diagram of the Pt-Sb system, as presented by (Duruselle and Feschotte 1991), is widely regarded as the most comprehensive and reliable representation of the phase relationships in this system. It was developed through a rigorous process involving differential thermal analysis, X-ray diffraction, and electron microprobe diagnostics, and its acceptance was subsequently endorsed by (Okamoto 1992; Itkin and Alcock 1996).

Experimental

Materials and methods of research

Experimental studies were conducted in platinum ampoules with a diameter of 5 mm and a length of 40–50 mm a hydrothermal high pressure apparatus at a temperature of 800 ± 2 °C and a total pressure of 190–200 MPa. The experimental parameters and initial solid phases are presented in Table 1.

The hydrogen pressure in the hydrothermal vessel, which has an internal diameter of 6–7 mm and is constructed from a heat-resistant stainless nickel alloy (EP-455), was set by a combination of copper and copper oxide, nickel and nickel oxide, and cobalt and cobalt oxide. The buffer mixture was placed in a container (tube) manufactured from titanium alloy VT-8, with both ends sealed. The experiment was maintained for a period of 24 to 48 h. Quenching of experimental products was performed within 3–5 min by airborne water cooling. The buffer container and Pt ampoule were removed from the cooled reactor. The ampoule containing the solution was inflated on a hot plate, then opened and the solutions with residual mineral phases were then removed

Table 1 Parameters of experiments on Pt-Sb intermetallics compound formation

Run No	T, °C	*P*, MPa	Solution, wt% NaF	Loaded phases (substances)	Buffer mixture	Run duration, hours
1	800 ± 2	200 ± 10	4.03	Synthetic roméite	Cu–(Cu_2O)?	24
2	800 ± 2	200 ± 10	10.0	Synthetic roméite	Cu–(Cu_2O)?	24
3	800 ± 2	200 ± 10	10.0	$Pt_{powder}+Sb_2O_5$	(Cu)–Cu_2O	48
4	800 ± 2	200 ± 10	10.0	$Pt_{powder}+Sb_2O_5+Z$	Co–CoO	48
5	800 ± 2	200 ± 10	4.03	$CaO+NaF+Sb_2O_5$	Cu_2O–CuO Co–CoO	24 48
6	800 ± 2	200 ± 10	4.03	$CaO+NaF+Sb_2O_5$	Cu_2O–CuO Ni–NiO	24 48

Z – seed plate, it was cut of the lower part of the platinum ampoule from the Experiment No. 1, consisting of Pt and an intermetallic compound Pt_5Sb

( ) – an insignificant amount of this component after the experiment

by washing with water into polypropylene test tubes. The solution was then separated from solid phases by centrifugation at 6000 rpm for 2–3 min. Na, Ca and Sb contents were determined in an aliquot of 4 ml of the solution using inductively coupled plasma methods (ICP-AES, ICP-MS). The precipitate was thoroughly washed to remove soluble salts, transferred to Petri dishes and dried in a cabinet at 100 °C. Composition of the crystals was determined using scanning electron microscopes (SEM) VEGA-TESCAN 5130MM, equipped with energy dispersive X-ray (EDX) microanalysis system (EMPA) with semiconductor Si(Li) detector INCA Energy 350, at a primary current of 0.12 nA at 20 kV and a beam diameter of 0.12 μm and Tescan Vega II XMU with INCA Energy 450 energy dispersive spectrometers with INCA PentaFET x3 and by X-ray diffraction using Bruker D2 Phaser digital X-ray diffractometer.

Influence of composition on Pt and Sb line shift in the product of formation was characterized by means of X-ray photoelectron spectrometer Kratos AXIS Ultra spectrometer with monochromatic Al-K_α radiation at 1486.6 eV (total resolution Ag $3d_{5/2}$ was about 0.48 eV). Spectra were calibrated using Ag $3d_{5/2}$ and In $3d_{5/2}$, C1s and O1s lines. The analyzed sample area was 700 × 300 μm. The pass energy is 40 eV for overview spectra and lines of low intensity or with significant shift due to charging; 20 eV for high intensity lines. The accumulation time per point was 0.1 s for individual element lines and 0.3 s for overview spectra (for 1 pass). The range of binding energies was determined to be within ± 10–15 eV relative to the position of the peak maximum. The measurement step exhibited a precision of 0.05 eV for spectra of individual element lines (0.1 eV for lines exhibiting a shift due to charging) and 0.2 eV for overview spectra.

Research results

Solid products of experiments

Oxygen buffers

In Experiments No. 1 and 2, conducted with roméite, the Cu_2O–CuO buffer mixture was reduced to pure copper, resulting in the formation of red crystals on the container surface. The reason for this is that the metal container in which the buffer mixture was placed was not of the same composition as titanium. In this case, it can be concluded that the oxygen fugacity in the reactor and ampoule was $fO_2 \leq 10^{-3.47}$ Pa.

In the Experiment No. 3, the buffer mixture, initially containing red Cu and black Cu_2O, after the experiments had a brick-red color and contained cuprite Cu_2O (PDF 002-1067). Subsequently, the fO_2 value ranged between $10^{-3.47}$ and 50 Pa.

In Experiment No. 4, in which the fO_2 was controlled by an external Co–CoO buffer, a decrease in the quantity of magnetic Co metal powder was observed. Taking into consideration the high rate of the reaction of cobalt oxidation to cobalt oxide, it can be assumed that fO_2 in the experiment corresponded to $10^{-10.21}$ Pa, i.e. Co–CoO buffer.

Experiments No. 5 and 6 were combined. In the initial 24-hour period, roméite was synthesized from a mixture of $CaO + NaF + Sb_2O_5$ in a 4 wt% NaF solution at $fO_2 = 50$ Pa (Cu_2O–CuO buffer). Then, ampoules with Rom, without opening, were placed in a new experiment for 48 h with containers which were containing Co–CoO and Ni–NiO buffers, respectively. X-ray phase analysis confirmed the presence of all components used in the buffer mixtures after the experiments were conducted.

Analysis of the inner surface and content of platinum ampoules after experiment

A platinum ampoule, exposed to fluoride solution containing 4.0 wt% NaF and roméite dissolution products at 800 °C, P_{total} = 200 MPa and $fO_2 \leq 10^{-3.47}$ Pa (Run No. 1), underwent visually noticeable changes. The lower part (about 1/3) of ampoule, which could contain a highly concentrated of salt solution (fluid phase L_2), underwent recrystallization, resulting in the formation of a conductive, brittle, platinum-colored solid phase on its surface. According to the SEM image (Fig. 1) taken with Backscattered Electrons (BSE) and Secondary Electrons (SE) detectors, the newly formed phase consists of homogeneous lamellar crystals with a polygonal shape. The structure of the plates is similar to platinum crystals grown from the gas phase (Strobel and Le Page 1981). According to SEM analysis (64 measurements) the phase has a composition of $Pt_{82.8\pm1.3}Sb_{17.2\pm1.3}$, which corresponds to the formula $Pt_{4.82}Sb$ or Pt_5Sb.

The upper part of the ampoule was pure platinum. Analysis of the cross section of the lower part of the ampoule (Fig. 2-a) showed that the antimony content in the platinum varied from 18 ± 1 at% (dots # 1–2) to 0 at% (dots # 20–22). According to the composition profile (Fig. 2-b), the inner layer of the ampoule up to 5–10 μm is represented by the Pt_5Sb compound, the middle layer from 10 to 45 μm is represented by the $Pt_{10}Sb$ compound and finally the outer part of the ampoule up to a depth of 155 μm is pure Pt.

In the Experiment No. 3 carried out in the Cu_2O cuprite stability region ($10^{-3.47}$ Pa ≤ fO_2 ≤ 50 Pa), in a solution containing 10 wt% NaF and a mixture of fine crystalline Sb_2O_5 and Pt, the inner surface of the platinum ampoule remained unchanged.

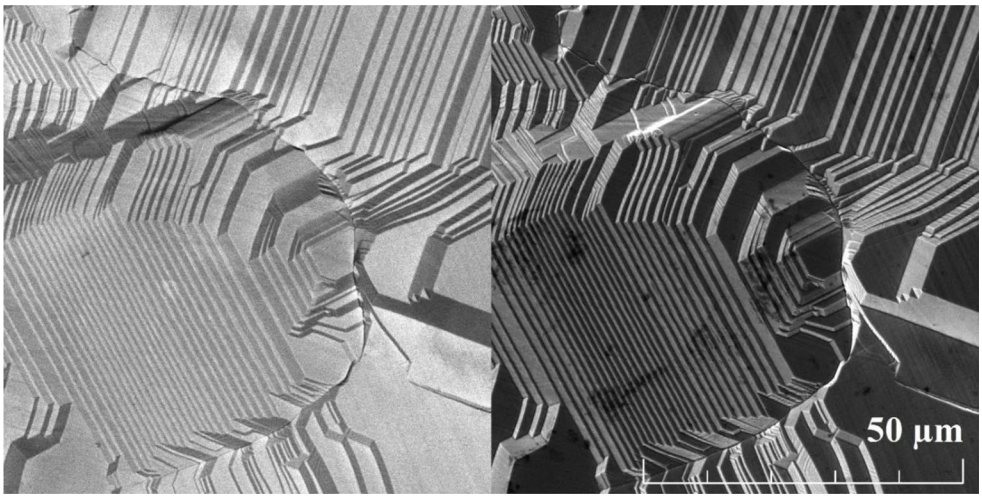

Fig. 1 Section of the inner lower part of a platinum ampoule after Experiment No. 1 at $fO_2 \leq 10^{-3.47}$ Pa

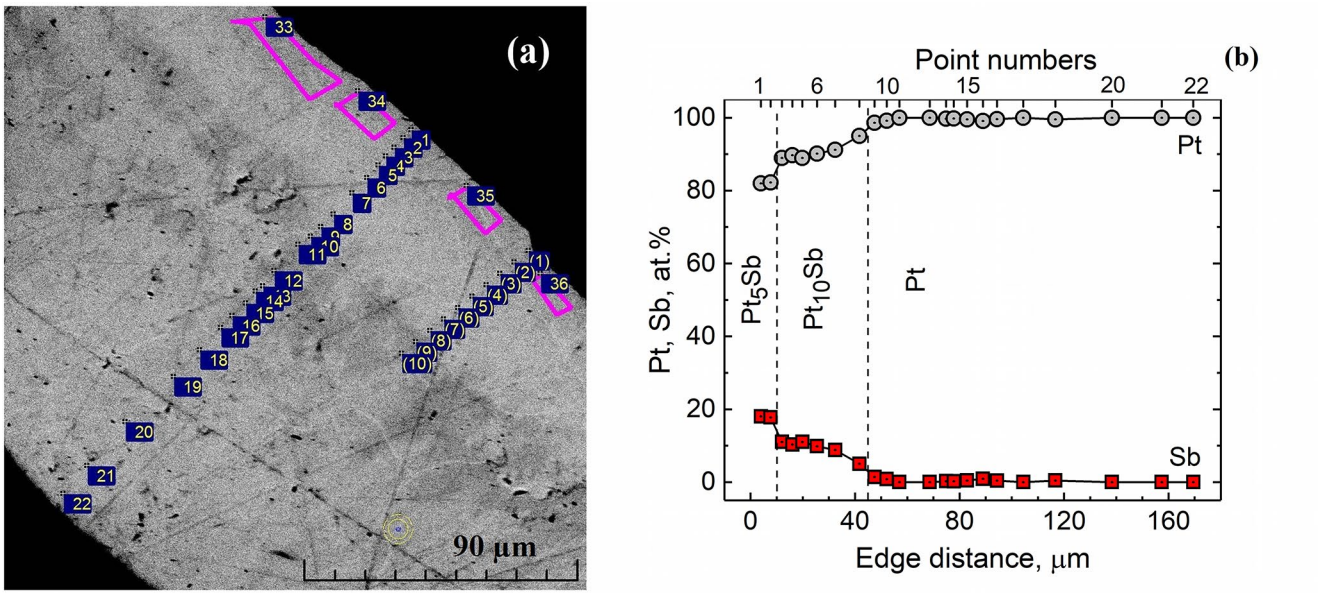

Fig. 2 (**a**) Points analyzed on the surface of the cross section of the lower part of the ampoule, the surface of which is shown in Fig. 1 (Run No. 1). (**b**) Profile of changes in the composition of a Pt ampoule in an experiment

The inner surface of the ampoule, where fO_2 was controlled by an external Co–CoO buffer (Run No. 4), was modified. The bottom of the ampoule, where the reaction mixture was located (h = 1 ÷ 2 mm), changed slightly. Above, approximately up to the middle of the ampoule the formation of platinum-antimony intermetallic occurred. The upper part of the inner surface of the Pt ampoule remained without significant changes and was represented by pure Pt.

The seed plate in the Experiment No. 4 has undergone significant changes and is thoroughly welded to the wall of the Pt tube. A polished sample in polystyrene for SEM analysis was prepared from a cutting containing part of the ampoule and a platinum-intermetallic seed plate. According to the SEM image (Fig. 3) obtained with the BSE detector, the Pt ampoule has undergone a change: inside the ampoule, the formation of a compound with a higher density (2–light color) than the original platinum (1–outside, pure Pt) has occurred. The thickness of the ampoule is 0.2 mm, therefore, at a height of ~ 1 cm from the bottom of the ampoule, the thickness of the newly formed layer is 50–60 microns.

The seed plate also had a thickness of 0.2 mm. During the experiment, the seed plate was coated on both sides to a depth of 50 µm with a compound of higher density (layers 4 and 5) than Pt (layer 3). The results of the analysis using an electron scanning microscope are presented in Table 2. The data obtained indicate that the interaction of platinum with antimony oxide at 800 ± 2 °C, 200 ± 10 MPa, in a solution containing 10 wt% NaF, fO_2 specified by Co–CoO buffer ($fO_2 = 10^{-10.21}$ Pa), leads to the formation of a solid solution

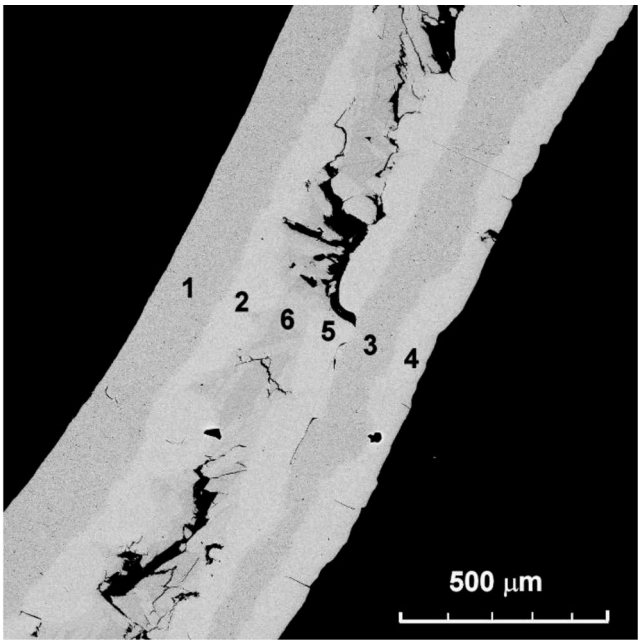

Fig. 3 SEM illustration of an intergrowth of a Pt ampoule with a seed (a cutout of a used Pt ampoule with a Pt_5Sb growth) captured with BSE detector after the Run No. 4. 1 – outer part of Pt ampoule; 2 – inner part of a Pt ampoule with an overgrown intermetallic compound of Pt and Sb; 3 – Pt seed containing 4 – Pt_5Sb; 5 – newly formed platinum-antimony intermetallic on the seed; 6 – melt containing platinum and antimony soldering the ampoule with the seed

Table 2 Results of the SEM analysis of the intergrowth of a pt ampoule with a seed (run. No 4)

Layer No	Test	Pt, at%		Sb, at%	
	numbers	Average	SD	Average	SD
1	3	100	0.3	0	0.3
2	3	90.8	4.3	9.2	4.3
3	3	100	0.3	0	0.3
4	3	90.8	0.6	9.2	0.6
5	3	89.9	1.4	10.1	1.4
6	12	69.2	4.4	30.8	4.4
$Pt_{10}Sb$ ISA-2 M	11	89.88	0.71	10.12	0.71
$Pt_{10}Sb$ PCL-2 M	12	89.79	0.48	10.21	0.48
$Pt_{10}Sb$ PISA-2 M	13	91.67	0.40	8.33	0.40
$Pt_{10}Sb$ PISA-3 M	5	90.73	0.41	9.27	0.41
$Pt_{10}Sb$ PCA-2 M	13	89.54	0.6	10.46	0.5
$Pt_{10}Sb$ PCA-3 M	4	89.73	0.76	10.27	0.76

PISA – polish inner surface of ampoule

PCA – polish cut of ampoule

PCL – polish cut of congealed liquid

SD – standard deviation

of antimony (9.2–10.1 at%) in platinum and a melt containing 30.8 ± 4.4 at% Sb and 69.2 ± 4.4 at% Pt.

During Experiment No. 4, using a mixture of the fine-crystalline reagents Pt and Sb_2O_5 and a seed plate under redox conditions set by a Co–CoO buffer, some formation in the form of spheroids was found in the ampoule. Four spheroids, in size of 70–150 μm, were pressed into a polystyrene tablet, polished (Fig. 4) and analyzed on an electronic scanning microscope. Apparently, the substance of the spheroids was heterogeneous. High antimony content in the products of the experiments indicates that the spheroids in the experiments were in the form of melts and during cooling, albeit rapid (up to 700 °C within 1–2 min), crystallization of $Pt_{10}Sb$ phase occurred in them and the composition of the melt was enriched with antimony, shifting to eutectic.

Since the composition of the spheroids is heterogeneous and the underlying layers can be illuminated, it is obvious that compositions with low antimony content (11–12 at%) may be overestimated, and those containing high concentrations of Sb (27–28 at%) can be underestimated. The actual composition of the phase maximally saturated with antimony should be 9.7 ± 0.8 at% Sb and 90.3 ± 0.8 at% Pt and composition of the eutectic melt at 630 °C should be 31 ± 4 at% Sb and 69 ± 4 at% Pt. Statistical processing of 53 SEM analyses is presented in Fig. 5.

Experiments No. 5 and 6 (see Table 1) were performed in two stages. First, the synthesis of roméite from a $CaO + NaF + Sb_2O_5$ mixture of stoichiometric composition was carried out at 800 °C, P_{total} = 200 MPa and fO_2 = 50 Pa (Cu_2O–CuO buffer). Subsequently, the ampoules were not opened and experiments were performed under the same *T*-*P* conditions but at fO_2 set by Co–CoO and Ni–NiO buffers, respectively.

According to SEM studies, the products of experiments under reducing conditions contained only skeletal forms of fluorite (Fig. 6). No solid Sb-containing phases were found in the bulk products of the experiments.

The platinum ampoule became brittle, especially on the inside, and fractures were observed when the surface was straightened. The inner surface of the ampoules underwent a significant change: polycrystalline formations appeared on it (Fig. 7). Figures 8-a and 9-a show SEM images of polished ampoule sections after the experiments and the test site. The composition of new formations at $fO_2 = 10^{-10.21}$ Pa (Co–CoO buffer) corresponds to 9.1 ± 1.4 at% Sb, 90.9 ± 1.4 at% Pt (19 analyses) and at $fO_2 = 10^{-8.81}$ Pa (Ni–NiO buffer) 11.9 ± 1.2 at% Sb, 88.1 ± 1.2 at% Pt (12 analyses). Profiles of compositions changes in the platinum and antimony during the experiments are presented in Figs. 8-b and 9-b. The data obtained indicate that at 800 °C, P_{total} = 200 MPa and H_2 pressure set by Ni–NiO and Co–CoO buffers, the oxide forms of antimony are reduced to Sb^0.

XRD analysis of powdered products of experiments

The powder products of the experiments were examined on a Bruker D2 Phaser X-ray diffractometer. In the products of

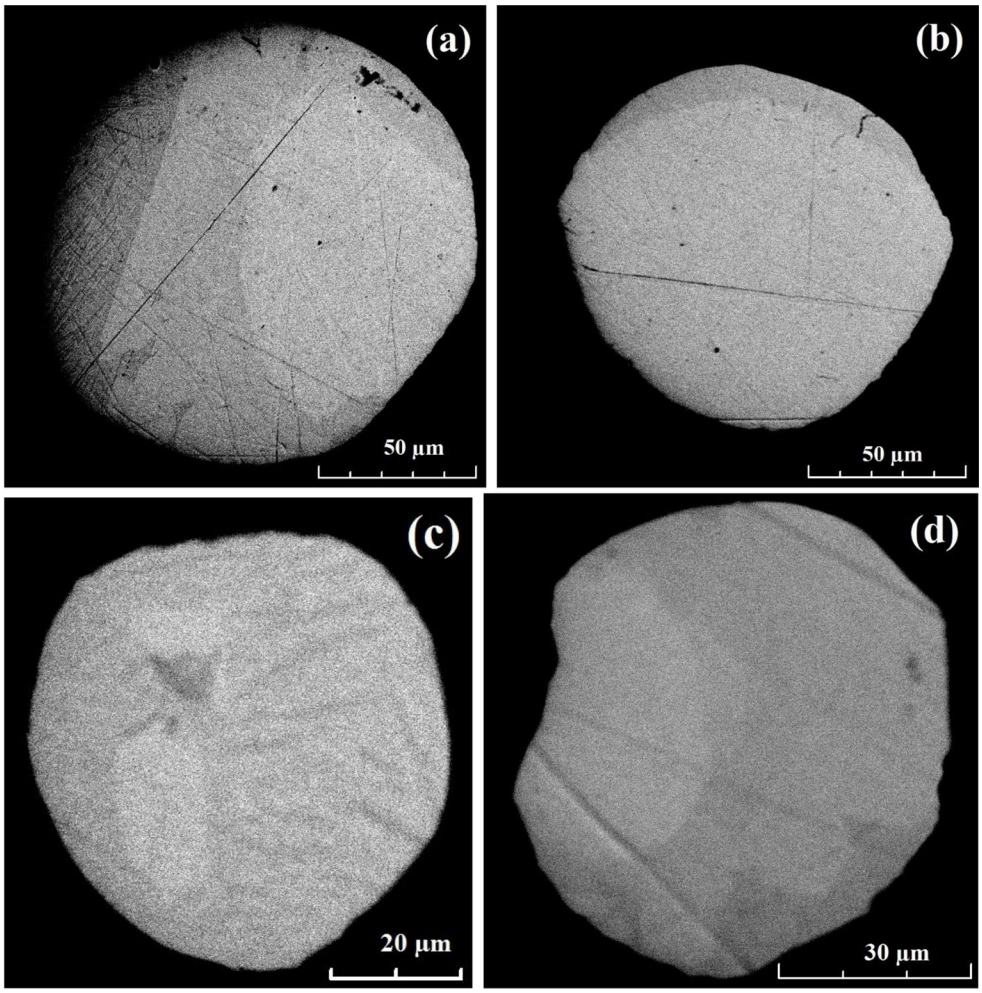

Fig. 4 (**a**, **b**, **c**, **d**) Platinum–antimony intermetallic spheroids formed in Experiment No. 4 at $fO_2 = 10^{-10.21}$ Pa (Co–CoO buffer)

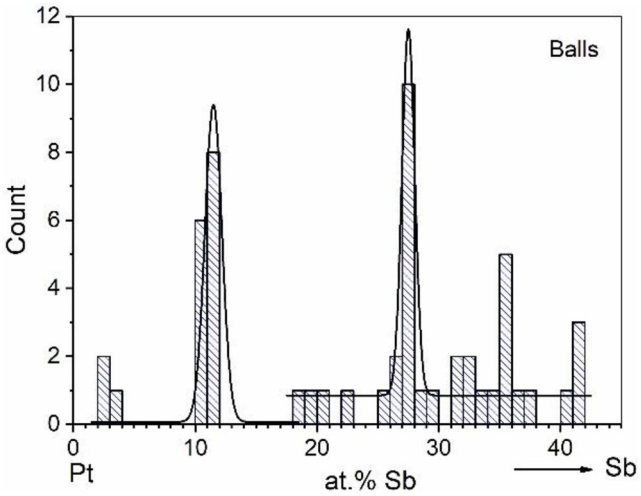

Fig. 5 Composition of platinum-antimony spheroidal intermetallics according to statistical analysis of 53 samples

Experiment No. 3 (Fig. 10), performed under redox conditions close to the Cu–Cu_2O buffer ($fO_2 = 10^{-3.47}$ Pa), along with platinum reflections (PDF 04-0802), weak lines characteristic of antimony oxides Sb_6O_{13} (PDF 21–0051) and Sb_4O_6 (PDF 76-1717) of the cubic system $Fd\bar{3}m$ with the unit cell parameters (LC) equal to $a = 10.304$ and 11.14 Å, respectively.

In the bulk products of Experiment No. 4 (Fig. 11), only intrinsic lines belonging to Pt (JCPDS PDF 00-004-0802) were observed.

The diffraction patterns of the products of Experiments No. 5 (and 6), as illustrated in Fig. 12, indicate the presence of fluorite. This suggests that roméite is not stable under redox conditions corresponding to Co–CoO and Ni–NiO buffers.

XRD analysis of the surface of Pt ampoules

Rounded cut samples from the bottom of the ampoule, which had gone through significant modification, were used for XRD analysis. The XRD of the sample (Run No. 1) imaged from the surface for 24 h is shown in Fig. 13. Due to the fact that the equipment which were used (D2 Phaser diffractometer) does not use circular rotation of the sample during the survey, the position of the sample relative to the

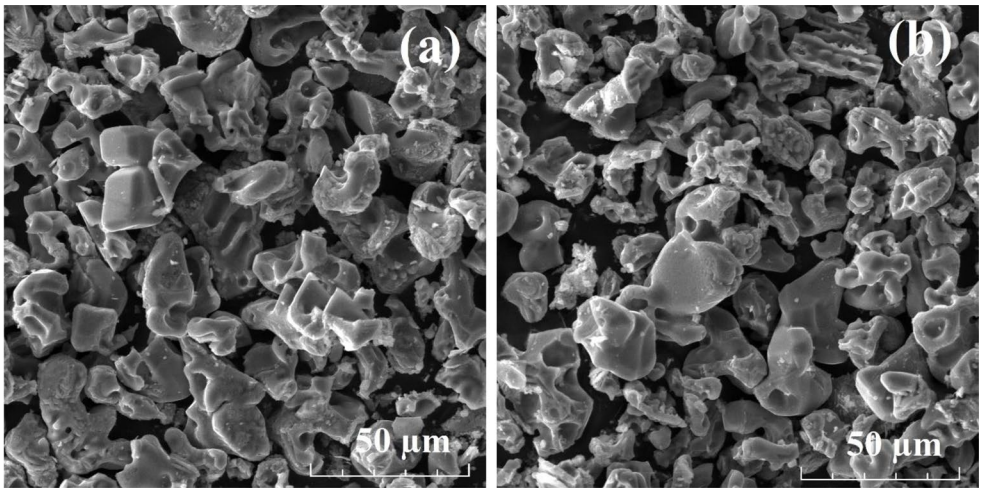

Fig. 6 The skeletal forms of fluorite that were formed during the dissolution of roméite in Experiments No. 5 and 6 at fO_2 given Co–CoO (**a**) and Ni–NiO (**b**) buffers

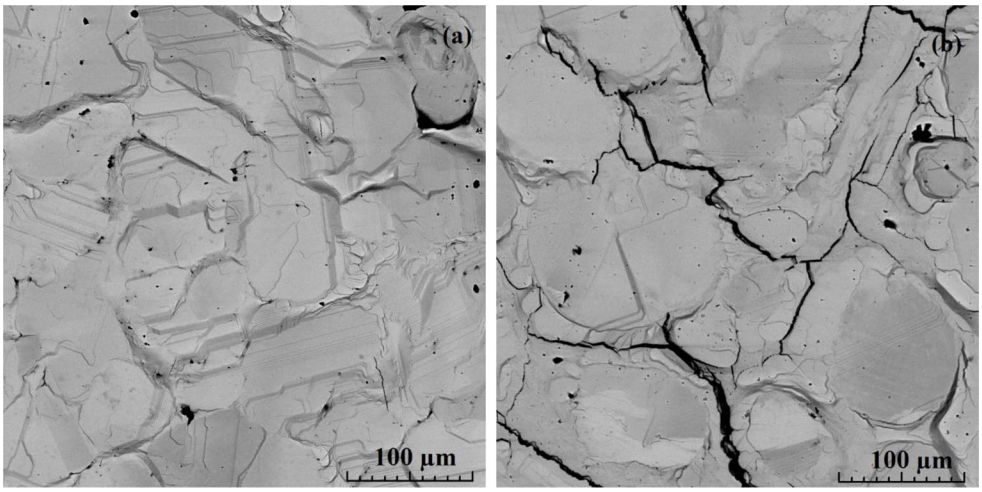

Fig. 7 The inner surface of Pt ampoules after Experiments No 5 and 6 performed at 800 °C, P_{total} = 200 MPa in a 1.0 *m*NaF solution and fO_2 given Co–CoO (**a**) and Ni–NiO (**b**) buffers

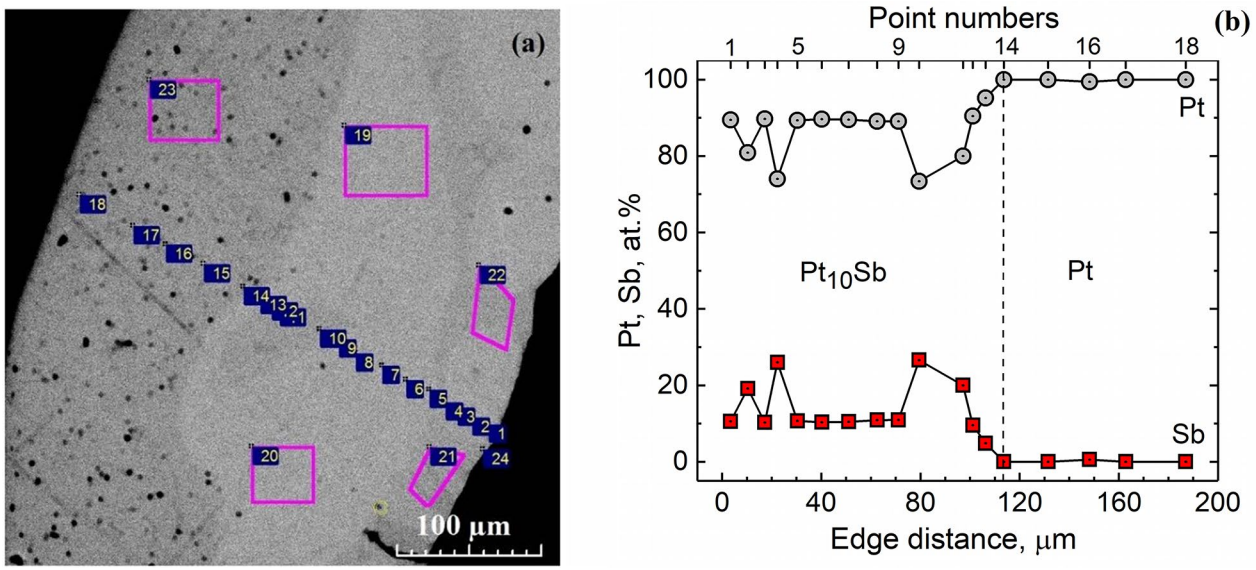

Fig. 8 (**a**) The analyzing points and surfaces of the cross-section of the lower part of the ampoule, the surface of which is shown in Fig. 8-a (Run No. 5). (**b**) The profile of changes in the composition of the Pt ampoule in an Experiment No. 5 carried out at fO_2 given a Co–CoO buffer

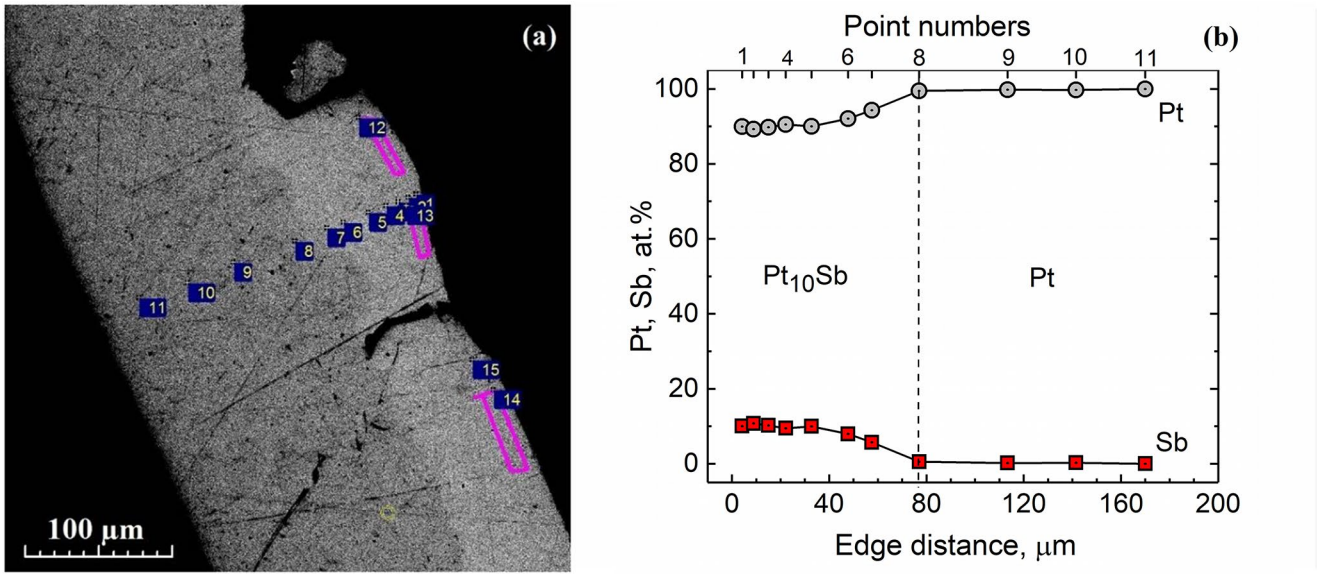

Fig. 9 (**a**) The analyzing points and surfaces of the cross-section of the lower part of the ampoule, the surface of which is shown in Fig. 8-b (Run No. 6). (**b**) The changes of the profile in the composition of the Pt ampoule in Experiment No. 6 carried out at fO_2 given a Ni–NiO buffer

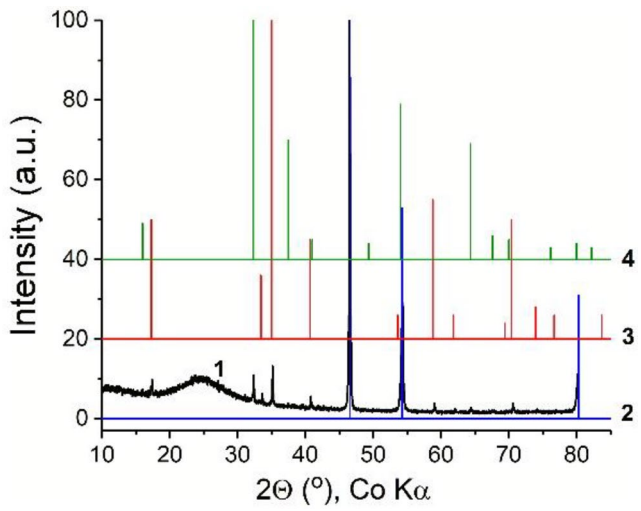

Fig. 10 XRD of the products of the Run No 3 on Pt-Sb intermetallics formation at fO_2 given a Cu–Cu_2O buffer. 1 – product of experiment; 2 – Pt (PDF 04-0802); 3 – Sb_6O_{13};(PDF 21-0051); 4 – Sb_4O_6 (PDF 11-694)

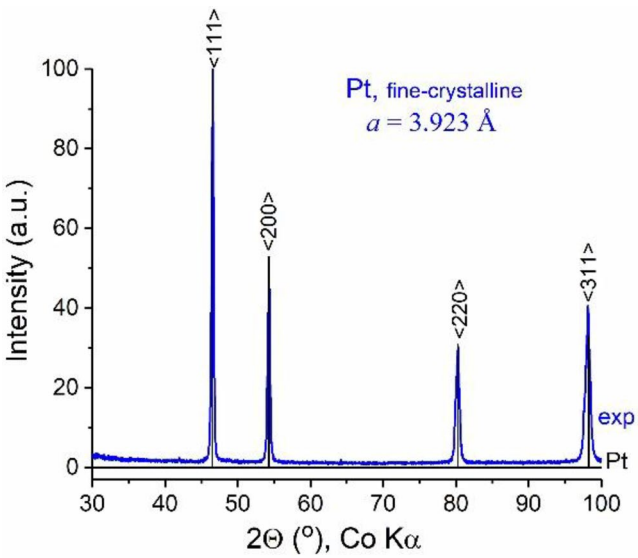

Fig. 11 XRD of dry products of the Run No. 4 on Pt-Sb intermetallics formation at fO_2 given a Co – CoO buffer. Exp – product of experiment; Pt – Pt (PDF 04-0802)

radiation source with a step of 60° (Fig. 14) was manually changed. As a result, it was detected that the intensity of characteristic lines depends on the angle of rotation. Analysis of the reflections showed that none of the intermetallic phases in the Pt-Sb system presented in the database corresponds to the obtained compound. In best way to be in line with calculated and experimental data which was obtained for hexagonal structure, *P6/mmm* with LC $a=b=4.56(4)$, $c=4.229(2)$ Å, $\alpha=\beta=90°$, $\gamma=120°$, V = 76.15 Å^3 and calculated density 23.92 g/cm^3.

In Experiment No. 2, according to the SEM analysis, an intermetallic with a composition of 90.3 ± 0.8 at% Pt and 9.7 ± 0.8 at% Sb was formed on the surface of the ampoule corresponding to the $Pt_{9.3}Sb$ compound of the cubic $Fm\bar{3}m$ symmetry (Fig. 15) with LC $a=3.943(3)$ Å. In contrast to pure Pt, the <111> and <200> lines, as well as the lines of the internal Si standard, are shown in Fig. 15, the <111> reflection of the $Pt_{9.3}Sb$ intermetallic practically did not appear.

In Experiments No. 5 and 6, the inner surface of the ampoule was coated with an intermetallic compound having an X-ray pattern identical to Pt_5Sb (Fig. 16). Under Ni–NiO buffer conditions, the <111> line did not appear in the

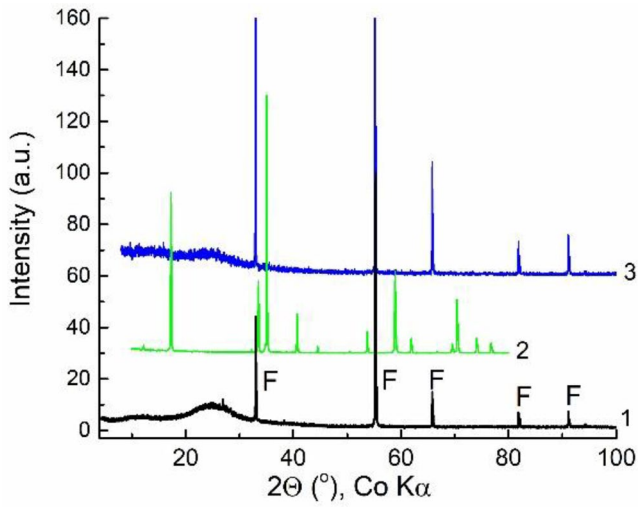

Fig. 12 XRD of the products of the Run No. 5 on Pt-Sb intermetallics formation at fO_2 given a Co–CoO buffer 1-product of experiment; 2-Rom; 3-Fl

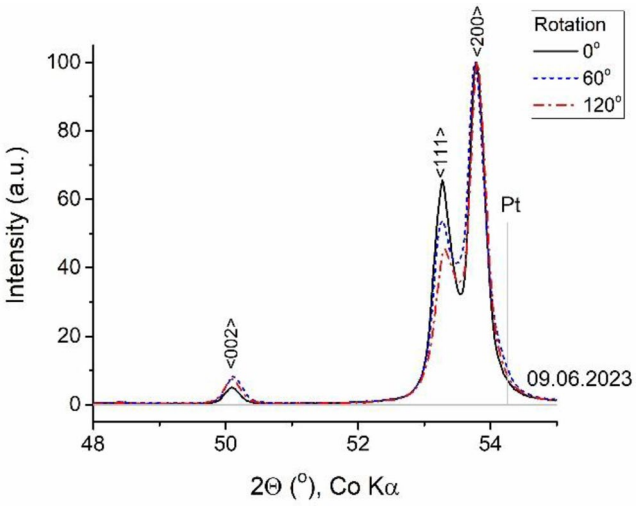

Fig. 14 The effect of rotation angle on the intensities of characteristic lines of Pt_5Sb (Run No. 1)

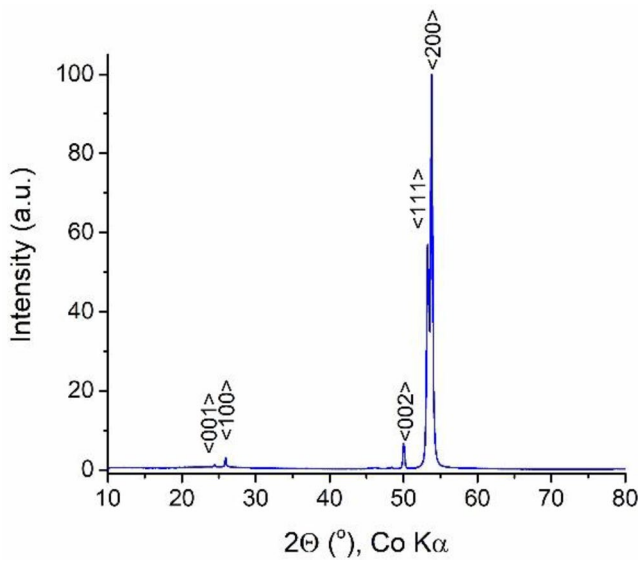

Fig. 13 XRD of a newly formed phase of composition $Pt_{5.00\pm0.05}Sb$, hexagonal symmetry, formed on the surface of a platinum ampoule in Experiment No. 1 on the roméite, $(NaCa)Sb_2O_6F$ solubility

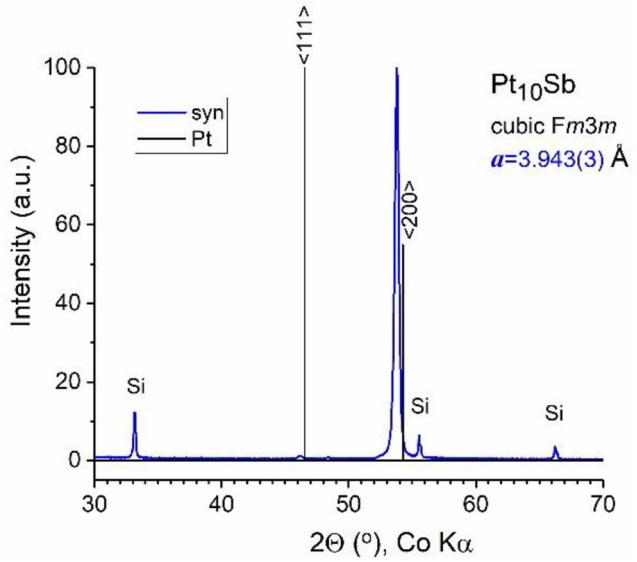

Fig. 15 XRD of the newly formed on the surface of the platinum ampoule phase of composition $Pt_{9.3\pm0.8}Sb$, cubic symmetry $Fm\bar{3}m$, in the Experiment No. 2 at $fO_2 \leq 10^{-3.47}$ Pa in the solution containing 10.0 wt% NaF. <111> and <200> are platinum lines (PDF 04-0802); Si-internal standard

spectrum, whereas under Co–CoO buffer, the broad line in the 53–54° 2Θ interval can be decomposed, using Lorentz Curve fitting, into two lines (Fig. 17): 53.34 (<111> 7%) и 53.80 (<200> 100%).

The platinum plate on the surface of which the formation of Pt_5Sb was observed (Experiment No. 1) was examined by X-ray diffraction three and four months later. The results of the noticeable changes are shown in Fig. 18. It was detected that the intensity that the intensity of the <111> reflex, was significantly decreased during exposure from 0 to 3 months at room temperature. The positions of other lines in the XRD spectrum (<001>, <100>, <002>, <200>) remained unchanged.

XPS surface analysis of Pt ampoules

The electronic structure and valence states of the prepared samples were investigated by X-ray photoelectron spectroscopy. Peaks of Pt4f, Pt4d, Pt4p, Sb3d, O1s, C1s were observed on the samples of compounds introduced into the electron spectrometer (Fig. 19). By etching with argon ions (4 keV, 1 min, about 1–2 nm was removed), surface

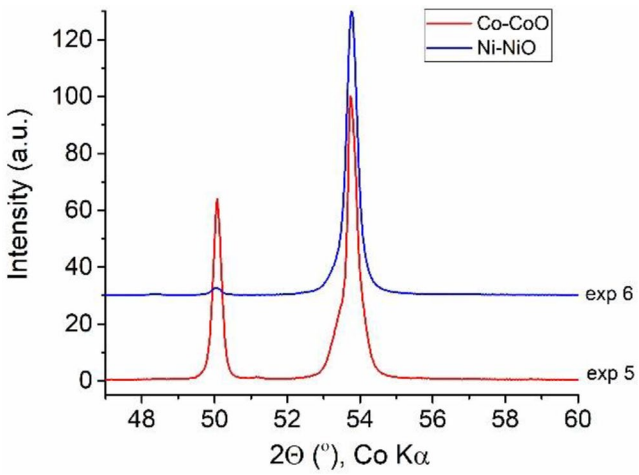

Fig. 16 XRD of the phases which were formed on the surface of the platinum ampoule in the Runs No 5 and 6 at Co–CoO and Ni–NiO buffers

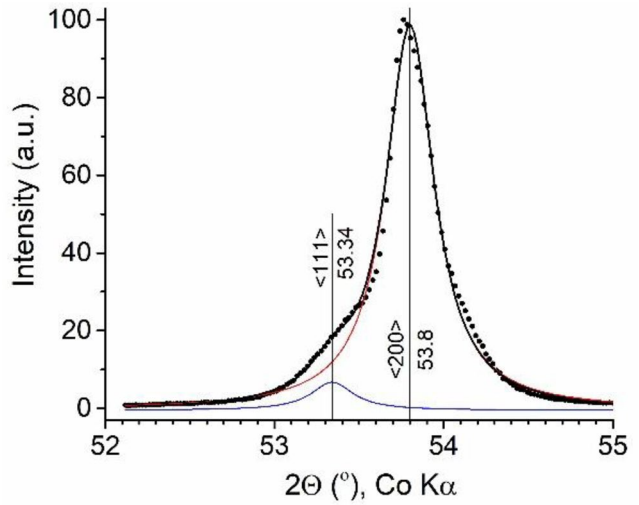

Fig. 17 XRD of the new phase from Experiment No. 5, formed on the surface of a platinum ampoule at Co–CoO buffer

adsorption impurities were removed and it allowed to clarify the features of the electronic structure of the compounds. The spectra of Pt4f lines and Sb3d demonstrated the shape of the lines and the binding energies of Pt4f–Sb3d with Pt4f – 70.61/73.96 eV and Sb3d – 528.03/537.46 eV characteristic of intermetallic compounds Pt-Sb, which also confirms the analysis of the valence band spectra, demonstrating the structure characteristic of metallic compounds with a noticeable intensity near the Fermi level and a density of states in the range 0–7 eV, which, according to the calculations given in (Zhang et al. 2020) is mainly due to the 5d states of platinum. Analysis of the survey spectra confirmed the elemental composition and stoichiometry of the Pt-Sb phases.

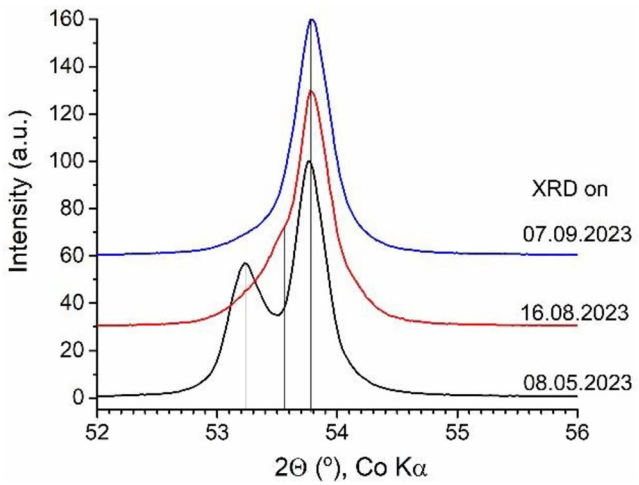

Fig. 18 XRD of the Pt_5Sb phase (Run No. 1) formed on the inner surface of the Pt ampoule, taken immediately after the Experiment No 1 on May 08, 2023, after 3 and 4 months

Discussion of the findings

The research findings indicate that the formation of platinum-antimony intermetallics has been observed in the zone most susceptible to hydrogen diffusion, specifically on the walls of the Pt ampoule. The main reactions that control the formation of Pt-Sb intermetallic compounds in the studies carried out may be as follows:

$$2x\ Pt + (CaNa)\,Sb_2O_6F + NaF = 2Pt_xSb + CaF_2 + Na_2O + 2.5\ O_2$$

and

$$2x\ Pt + Sb_2O_5 = 2\ Pt_xSb + 2.5\ O_2.$$

The interaction of both roméite and antimony pentoxide with platinum leads to the release of oxygen, which prevents the formation of new compounds with a suspension of platinum powder inside the ampoule. Furthermore, the seed containing Pt_5Sb could lose part of the antimony, transforming into face-centered cubic phase of the $Pt_{10}Sb$ composition (Table 2).

The walls of the platinum ampoule, having high permeability to hydrogen at high temperatures, are able to pass inside a sufficient amount of H_2 formed inside the hydrothermal reactor due to the buffer reaction

$$Me + H_2O = MeO + H_2,$$

where Me – Co or Ni.

Dissolved Sb(V) particles are reduced to Sb^0 on the inner surface of the ampoules and interact with Pt to form an intermetallic melt. Since the studies were carried out in the

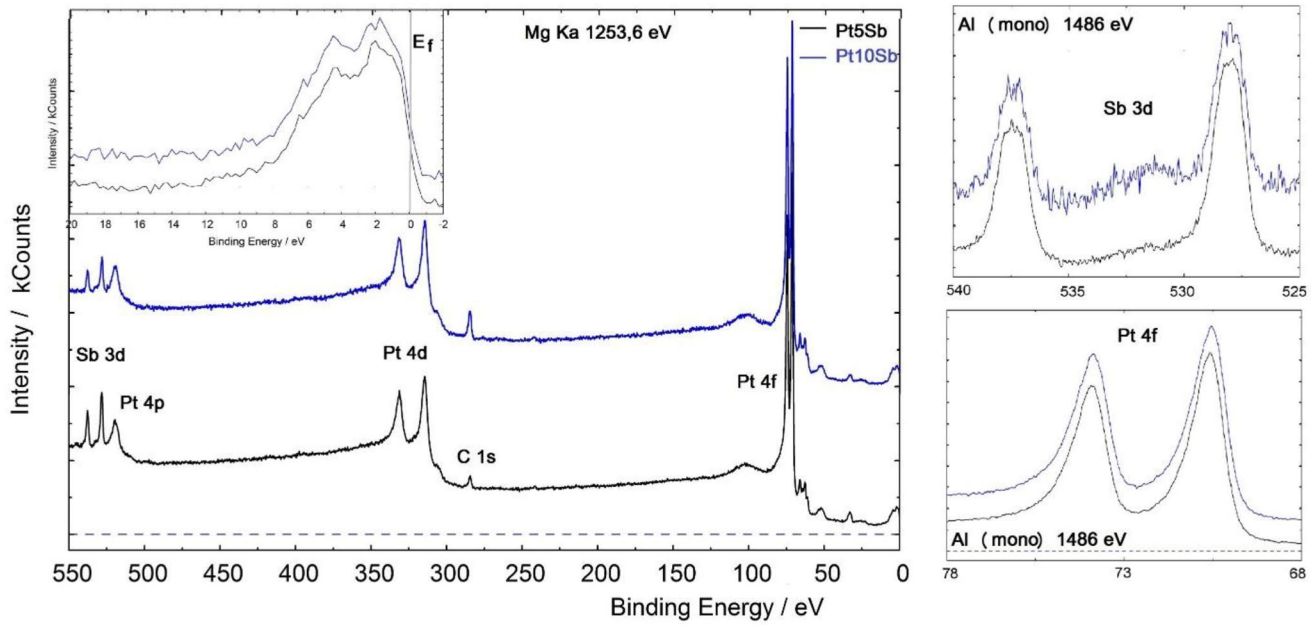

Fig. 19 XPS spectra of core levels and valence band of synthesized Pt-Sb compounds after ion bombardment

field of fluid miscibility of the NaF-H_2O system, the amount of dissolved antimony in the L_1 and L_2 fluid phases will be different. As stated by (Redkin et al. 2024), the solubility of roméite in the L_1 and L_2 phases is 0.4 and 2.1 wt% Sb, respectively. It follows that a highly concentrated solution located in the lower part of the ampoule will contain antimony in a quantity five times greater than that present in a solution situated in the upper part. In consequence, during the process of deposition of antimony, the lower section of the internal surface of the ampoule will undergo greater corrosion than the upper section. In Experiment No. 4, where a Pt seed containing Pt_5Sb and a mixture of Pt and Sb_2O_5 powders were used, the platinum ampoule and the seed plate were soldered to each other. The soldering alloy contained 30.8 ± 4.4 at% Sb and 69.2 ± 4.4 at% Pt (layer 6 in Fig. 2; Table 2). Similar concentrations of Sb and Pt were also obtained for spherical formations (see Fig. 5).

The phase diagram in the Pt-Sb system has been the subject of repeated clarification in the works of (Nemilow and Woronow 1936; Hansen 1936; Hansen and Anderko 1958; Bhan et al. 1969; Srivastava et al. 1972; Massalski et al. 1986; Kim 1988; Kim and Chao 1990; Kim 1993; Lyakishev 2000; Durussel and Feschotte 1991). According to (Okamoto 1992; Itkin and Alcock 1996), the data presented in (Durussel and Feschotte 1991) are the most reliable. Later, (Liu et al. 2013), summarizing the available data, performed thermodynamic calculations in the Pt-Sb system. According to their calculations, the Pt_5Sb phase (cubic, $Fm\bar{3}m$) is a solid solution that should be stable in the temperature range from 560 to 860 °C and its composition can vary from 15.5 to 18.9 at% Sb. This composition range is attributed in (Durussel and Feschotte 1991) to a solid solution of the $Pt_{4+x}Sb$ phase, cubic system fcc, but its stability is limited to the range 560–748 °C. Some researchers, apparently due to insufficient experimental data, do not consider this phase or attribute it to a tetragonal structure similar to Pt_4Sb (Kim and Chao 1990; Kim 1993). The phase diagrams of the indicated authors in the range 0 to 50 at% Sb, which are of interest for our research, are presented in the supplementary material.

The results of our research are most consistent with the data of (Kim and Chao 1990; Kim 1993). The obtained Pt_5Sb phase containing 82.8 ± 1.3 at% Pt and 17.2 ± 1.3 at% Sb, presumably of hexagonal crystal system, seems to be metastable at 800 °C and it should decompose into cubic phase of composition 90.1 ± 0.8 at% Pt and 9.9 ± 0.8 at% Sb ($Pt_{9.2\pm0.7}Sb$) and the melt containing 26.4 ± 0.9 at% Sb and 73.6 ± 0.9 at% Pt. Reducing the temperature to 600 °C may stabilise the stability of the $Pt_{5-x}Sb$ phase with tetragonal structure (Kim 1988).

Data from SEM analyses of sections of platinum ampoules (Figs. 2, 4, 9-a and 10-a) after the experiments allow us to propose a mechanism for the formation of intermetallic compounds in the Pt-Sb system. As can be seen from the scans of polished samples (Figs. 3, 9-b and 10-b), the depth of penetration of antimony into the walls of the Pt ampoules ranges from 45 µm (Run No. 1) to 100 µm (Run No. 5) and depends on fO_2. In Experiment No. 1 ($fO_2 \leq 10^{-3.47}$ Pa), the composition of the intermetallic compound in the surface layer up to 8 µm corresponds to the Pt_5Sb compound. Further, from 10 to 40 µm, the content

of antimony practically does not change and corresponds to the composition of $Pt_{10}Sb$. Deeper than 45 μm is pure Pt.

In Experiment No. 6 ($fO_2 = 10^{-8.81}$ Pa, Ni–NiO buffer), the depth of Sb penetration into the walls of the Pt ampoule is 60 μm. The composition of intermetallic phase corresponds to the formula $Pt_{90}Sb_{10}$.

In Experiment No. 5 ($fO_2 = 10^{-10.21}$ Pa, Co–CoO buffer), inhomogeneities of the intermetallic composition were observed in the range from 0 to 100 μm. The majority of the analyses (8 and 9) are in accordance with the $Pt_{90}Sb_{10}$ compound, while four sampling locations exhibit anomalous data: two samples provide the composition of $Pt_{80}Sb_{20}$ while the other two yield $Pt_{74}Sb_{26}$ (Fig. 9-б).

The experimental data and the results of XRD studies of newly formed Pt-Sb phases are insufficient for conclusions about the influence of fO_2 on the composition of intermetallics. As Pt_xSb intermetallics with cubic structure represent solid solutions of Sb^0 in Pt^0, their composition should be independent of fO_2 (fH_2). The primary factor influencing the composition of the solid solution of the cubic Pt_xSb phase is the ratio of Pt to Sb, the temperature, and potentially the total pressure.

Taking into account the significant penetration depth of antimony into the platinum ampoule, Figs. 2, 4, 9 and 10, the relative constancy of the composition, the high content of antimony in the fcc phase and the high probability of the formation of melt platinum with antimony, the following mechanism can be proposed for the formation of intermetallics of different compositions in Experiments No. 1, 3–5. Hydrogen from outside the Pt ampoule easily penetrates through its walls and causes the reduction of dissolved particles and complexes of Sb^{5+} to Sb^0. The growth of fH_2 inside the ampoule leads to the appearance of Sb^{3+} particles in the solution, which significantly increases the solubility of roméite and antimony pentoxide in solution, especially in the L_2 phase. Antimony deposited on the inner surface of the ampoule as Sb^0 forms an intermetallic melt with Pt^0 containing 28 to 35 at% Sb, which easily wets the surface of the ampoule (Straumal 2004) and starts the diffusion process of Sb^0 in the platinum ampoule. At 800 °C and with experiments lasting between 24 and 48 h, the depth of penetration of antimony into platinum can be considerable. Unfortunately, there is no data available on the diffusion of Sb^0 to Pt^0 with these specified parameters. The covalent atomic radii Pt^0 and Sb^0 are equal to 136(5) and 139(5) pm (Emsley 1998; Cordero et al. 2008), i.e. they have similar values. Therefore, self-diffusion data of the radioactive isotope ^{197}Pt in a Pt crystal can be used to estimate the diffusion depth (Rein et al. 1978). According to Fick's 2nd law, the concentration of C^T (at%) of the ^{197}Pt isotope at the diffusion front of depth X (cm) depends on the initial concentration of isotope C^T (at%) dwell time (t, sec) and the self-diffusion coefficient (D^T, $cm^2 \cdot sec^{-1}$) are determined by the formula:

$$C^T = \frac{C_0^T}{\sqrt{\pi\, D^T}} \exp\left(-\frac{X^2}{4D^T t}\right)$$

Substituting into this equation the value $D^T = (1.2 \pm 0.2) \cdot 10^{-14}$ $cm^2 \cdot sec^{-1}$ (Rein et al. 1978), the time of the experiment 172,800 s (= 48 h), we can calculate that the diffusion front or self-diffusion depth of the ^{197}Pt isotope is $X = 3$ μm. But since the covalent radius of Sb^0 is larger than that of Pt^0, it can be assumed that at 800 °C in 48 h the depth of antimony diffusion in platinum will not exceed 3 μm.

Obviously, there is another mechanism of antimony penetration into platinum besides diffusion. The intermetallic melt wets the surface of the ampoule and creates a wedging pressure, easily penetrates through microcracks, dislocations and other disturbances in the platinum under stress changes (in the experiments there are temperature and pressure fluctuations) and interacts with Pt atoms. I.e., the Rebinder effect (Rebinder 1928; Rebinder and Shchukin 1973; Malkin 2012) occurs, resulting in the destruction of the platinum layer due to the action of the surfactant Pt-Sb melt. The platinum ampoule was subjected to physical stress at the outset of the experiment (heating and overpressure relief) and throughout the experiment itself. This is due to the fact that the ampoule is constantly subjected to insignificant pressure changes as a result of the peculiarities of reactor heating (heating on-off mode). This facilitates penetration of the Pt-Sb melt deep into the Pt ampoule, which has significant cracking associated with the peculiarities of its manufacture.

Obviously, the intermetallic phase containing the maximum amount of Sb, i.e. $Pt_{90}Sb_{10}$ (Durussel and Feschotte 1991), begins to crystallize at the boundary of platinum (which has the same cubic structure) and the melt in the case of total antimony deficiency in the system:

$200Pt^S + Pt_{70}Sb_{30}{}^L \Rightarrow 3Pt_{90}Sb_{10}{}^S$,

i.e. 1 mol of melt will require 2 moles of platinum. According to the available data as well as our XRD studies, the newly formed $Pt_{90}Sb_{10}$ phase occupies a larger molar volume than Pt_{100}. The crystallization of $Pt_{90}Sb_{10}$ will lead to the destruction of the wall of the Pt ampoule and a decrease in the volume of the melt.

Conclusions

Studies performed in NaF-containing hydrothermal fluids have shown that the oxide compounds Sb^{5+} are unstable at 800 °C, P_{total} = 200 MPa and fO_2 (fH_2) specified by Co–CoO and Ni–NiO buffers interact with the ampoule

Pt material, forming antimony intermetallics with platinum on the inner surface of the ampoule. The formation of the following intermetallics was established through the analysis of data obtained from electronic microscope studies: $Pt_{90.3\pm0.8}Sb_{9.7}$ (~$Pt_{10}Sb$), $Pt_{82.8\pm1.3}Sb_{17.2}$ (~Pt_5Sb) and $Pt_{69.2\pm4.4}Sb_{30.8}$. The compound Pt_5Sb, which is presumed to be hexagonal *P6/mmm* crystal system with unit cell parameters $a=b=4.56(4)$, $c=4.229(2)$ Å, $\alpha=\beta=90°$, $\gamma=120°$, forms a thin film (≤ 10 μm) on the Pt surface and appears to be a metastable phase. The intermetallic compound $Pt_{69}Sb_{31}$ is a rapidly cooled melt of an appropriate composition.

The XPS spectra of Pt4f and Sb3d lines demonstrated the shape of the lines characteristic of intermetallic compounds Pt-Sb, which also confirms the analysis of the valence band spectra, demonstrating the structure of metallic compounds with a noticeable intensity near the Fermi level and a density of states in the range 0–7 eV, which is mainly due to the 5d states of platinum. Analysis of the survey spectra confirmed the elemental composition and stoichiometry of the Pt-Sb phases.

A mechanism for deep penetration of Sb into the walls of the Pt ampoule is proposed.

Supplementary Information The online version contains supplementary material available at https://doi.org/10.1007/s00269-024-01299-0.

Acknowledgements The authors thank N.A. Drozhzhina (Korzhinskii Institute of Experimental Mineralogy, Russian Academy of Sciences) for XRD analyses of the solid experimental products. We are thankful to the reviewers for discussion and valuable comments and to the scientific editor and the editors of the journal for attention to this manuscript. The XPS investigations were carried out using the equipment of the Collective Use Center of the ISSP RAS.

Author contributions Alexander F. Redkin carried out experimental studies, investigated the newly formed phases, and wrote the paper. Alexey N. Nekrasov took SEM images of Pt-Sb compounds, prepared illustrations and investigated their composition. Andrey M. Ionov and Rais N. Mozhchil performed the studies on x-ray photoelectron spectrometer Kratos AXIS Ultra spectrometer and presented the results. Andrey D. Podobrazhnykh conducted XRD studies, calculated X-ray parameters of newly formed phases their density and unit cell volumes.All authors reviewed the manuscript.

Funding This work was supported by the Fundamental Research Program in the Russian Federation, project FMUF–2022-0002, FMUF–2022-0003, ISSP RAS state assignment, and by the Russian Federation represented by the Ministry of Education and Science of the Russian Federation Project No. 13.1902.24.44, Agreement No. 075–15-2024–641. No additional grants to carry out or direct this particular research were obtained.

Data availability No datasets were generated or analysed during the current study.

Declarations

Competing interests The authors declare no competing interests.

References

Bhan S, Gödecke T, Schubert K (1969) Konstitution Einiger Mischungen des platins mit b-elementen (B = sn, Sb, Te). J Less-Common Met 19(2):121–140. https://doi.org/10.1016/0022-5088(69)90027-7

Cordero B, Gómez V, Platero-Prats AE, Revés M, Echeverría J, Cremades E, Barragán F, Alvarez S (2008) Covalent radii revisited. Dalton 21:2832–2838. https://doi.org/10.1039/b801115j

Durussel Ph, Feschotte P (1991) Les Systèmes binaires Pd-Sb et Pt-Sb. J Alloy Compd 176(1):173–181. https://doi.org/10.1016/0925-8388(91)90023-O

Emsley J (1998) The Elements, 3rd edition. Oxford University Press, 300 p

Hansen M (1936) Der Aufbau Der Zweistofflegierungen. Eine Kritische Zusammenfassung. Springer-, Berlin, Heidelberg, p 1100. https://doi.org/10.1007/978-3-642-47516-0

Hansen M, Anderko K (1958) Constitution of binary alloys, 2 edn. McGraw-Hill Book Co., NY, nd ed., New York, p 1305

Itkin VP, Alcock CB (1996) The Pt-Sb (platinum-antimony) system. J Phase Equilib 17:356–361. https://doi.org/10.1007/BF02665564

Kim W-S (1988) Phase constitution of the Pt-Sb system. J Korean Inst Met 26:378–384

Kim W-S (1993) Phase and phase equilibria in the Pt-Sb system. J Korean Inst Min Geol 26(3):18–24

Kim W-S, Chao GY (1990) Phase relations in the system Pt-Sb-Te. Can Mineral 28:675–685

Liu J, Zhang Y, Guo C (2013) Thermodynamic Assessment of the Pt-Sb system. Int J Nonferrous Metall 2:95–99. https://doi.org/10.4236/ijnm.2013.23013

Lyakishev (2000) State diagrams of binary metallic systems (2000) Reference book: In 3 volumes: V. 3. Book. 2. Under the general ed. N.P. Lyakishev. Moscow: Mechanical Engineering, 2000. 448 p. ISBN 5-217-02932-3

Malkin AI (2012) Regularities and mechanisms of the Rehbinder's effect. Colloid J + 74 2223–238. https://doi.org/10.1134/S1061933X12020068

Massalski TB, Murray JL, Bennett LH, Baker H (1986) Binary Alloy Phase Diagrams, Vol 1 and 2, American Society for Metals, Metals Park, OH. 2224p

Nemilow WA, Woronow NM (1936) Über Legierungen Des Platins Mit Antimon. Z Anorg Allg Chem 226(2):177–184. https://doi.org/10.1002/zaac.19362260211

Okamoto H (1992) Pt-Sb (Platinum-Antimony). J Phase Equilib 13(5):580–581. https://doi.org/10.1007/BF02665778

Rebinder PA (1928) On the influence of surface energy change on cleavage, hardness and other properties of crystals. VI Congress of Russian physicists. Gosizdat, Moscow, p 29

Rebinder PA, Shchukin ED (1973) Surface phenomena in solids during the course of their deformation and failure. Sov Phys Uspekhi 15(5):533–554. https://doi.org/10.1070/pu1973v015n05abeh005002

Redkin AF, Ionov AM, Nekrasov AN, Mozhchil RN, Reutova OV (2020) Structural aspects of pyrochlores stability: influence of the cations in [8]a, [6]B positions and lattice parameters. Phys Chem Min 47:47. https://doi.org/10.1007/s00269-020-01114-6

Redkin AF, Kotova NP, Shapovalov YB, Nekrasov AN (2024) Study of roméite solubility in the fluid immiscibility region of the NaF–H_2O system at 800°C, 200 MPa. Geochem Int 62(4):384–392. https://doi.org/10.1134/S0016702923700155

Rein G, Mehrer H, Meier K (1978) Diffusion of ^{197}Pt and ^{199}Au in platinum at low temperatures phys stat sol 45(1):253–261. https://doi.org/10.1002/pssa.2210450130

Srivastava PK, Giessen BC, Grant NJ (1972) A noncrystalline Pt-Sb phase and its equilibration kinetics. Metall Trans 3:977–982. https://doi.org/10.1007/BF02647675

Straumal BB (2004) Phase transitions at grain boundaries. Liquid-phase and solid-phase wetting, pre-wetting, pre-melting. Study guide. Moscow: MISIS, 2004. 80 p

Strobel P, Le Page Y (1981) Growth of large platinum crystals by chemical vapor transport. J Cryst Growth 54(2):345–346. https://doi.org/10.1016/0022-0248(81)90480-2

Zhang Y, Qiao M, Huang Y, Zou Y, Liu Z, Tao L, Li Y, Dong C-L, Wang S (2020) In situ exfoliation and pt deposition of Antimonene for Formic Acid Oxidation via a predominant dehydrogenation pathway. AAAS Res Article ID 5487237:PMC7054718. https://doi.org/10.34133/2020/5487237